Influence of the preparation method in the metal-support interaction and reducibility of Ni-Mg-Al based catalysts for methane steam reforming

Lola Azancot, Luis F. Bobadilla, José L. Santos, José M. Córdoba, Miguel A. Centeno and José A. Odriozola*

Instituto de Ciencia de Materiales de Sevilla – Departamento de Química Inorgánica, Centro mixto CSIC – Universidad de Sevilla, Av. Américo Vespucio 49, 41092 Sevilla (Spain)

Corresponding author (*): lola.azancot@icmse.csic.es

Abstract

Ni-Mg-Al based catalysts were prepared using different preparation methods (impregnation, impregnation-coprecipitation and coprecipitation) and tested in steam reforming of methane. The differences observed in catalytic activity were directly correlated to the physicochemical properties and the different degree of Ni-Mg-Al interaction. The reducibility results showed that the catalyst prepared by the impregnation-coprecipitation method presented the most optimal metal-support interaction to reduce the NiO preserving the Ni^0 particles highly dispersed on the support surface. These results demonstrate that the structure and catalytic performance of Ni-Mg-Al based catalysts can be tuned by controlling the metal-support interaction through of the preparation method.

Keywords: *Ni-Mg-Al catalysts; metal-support interaction; reducibility; methane steam reforming; H_2 production.*

1. Introduction

The most important procedure for large scale manufacture of hydrogen for synthesis of ammonia, methanol, and other petrochemicals is the catalytic steam reforming of natural gas [1, 2]. Methane is the majority component of natural gas and the main reaction that takes place in the steam reforming process is:

$$CH_4 + H_2O \rightarrow CO + 3H_2 \qquad \Delta H^0_{298K} = 205.8 \text{ kJ mol}^{-1} \qquad (1)$$

This reaction is highly endothermic and requires high temperatures (700 – 900 ºC) to achieve high conversions because of the strong C-H bond of methane molecule [3]. An excess of steam is typically used to promote the methane conversion and favour the gasification of the carbonaceous deposits formed during the reaction [4]. Moreover, under these conditions the water gas shift (WGS) reaction also takes place producing further hydrogen and CO_2 according to the following equation:

$$CO + H_2O \leftrightarrow CO_2 + H_2 \qquad \Delta H^0_{298K} = -41 \text{ kJ mol}^{-1} \qquad (2)$$

Ni-based catalysts have been extensively proved as efficient catalysts for steam reforming of methane due to its excellent C-H breaking ability. However, these kind of catalysts are prone to deactivation by coke deposition and metal sintering. Different strategies have been proposed to overcome these difficulties. For instance, it has been demonstrated that the addition of a basic metal oxides such as MgO facilitates the coke removal through the gasification of carbon deposits on the catalyst surface [5]. Conventionally, magnesium aluminate spinel ($MgAl_2O_4$) is used as an optimal catalyst support for steam reforming of methane due to its low acidity and excellent thermal stability [6, 7]. Guo et al. [8] reported that the use of $MgAl_2O_4$ as a support for Ni-based catalysts produce highly dispersed active Ni species very active and resistant to coke formation. Coleman et al. [9] reported that $MgAl_2O_4$ spinel compound exhibits moderate acidic-basic sites strength compared to the pure oxide supports and the moderation of the acid–base properties enhances the activity, selectivity, and stability of the catalyst.

In this sense, the utilization of Ni-Mg-Al mixed oxides as catalysts for reforming reactions has been also widely investigated due to their particular properties [10-13]. Several parameters such as composition or calcination temperature can influence notably the catalytic properties of Ni–Mg–Al-mixed oxides existing a compromise between the reducibility of Ni and the acid-base properties of material. Lin et al. [14] studied the effect of Ni loading in a series of catalysts prepared from Ni–Mg–Al layered double hydroxides and obtained an efficient catalyst with 12 wt.% of Ni for dry reforming of methane. Pérez-López et al. [15] evaluated the influence of the catalyst composition and the influence of the thermal treatment on the properties of Ni–Mg–Al based catalysts for CO_2 reforming of methane. They found an optimal Ni/Mg ratio of $1 < Ni/Mg \leq 5$ and the results revealed that reduction temperature has a strong influence in the catalytic activity and the selectivity. In other study, Li et al. [16] studied the dependence of the composition and reduction pretreatment conditions on the catalytic performance of catalysts containing Ni, Mg and Al. The best catalytic results were obtained for an optimized molar composition of Ni/Mg/Al = 9/66/25. In addition, Katheria et al. [17] also investigated the effect of calcination temperature on the physico-chemical and catalytic properties of $Ni/MgAl_2O_4$ catalyst for steam reforming of methane. They stated that an increase in the calcination temperature resulted in a decrease in the Ni crystallite size and the degree of reduction which was attributed to formation of a solid solution of NiO with the support.

It is well established in the literature that the metal-support interaction plays a crucial role in the catalytic performance of metal supported catalysts. An optimal metal-support interaction can increase the number of catalytically active sites and prevent the metal sinterization enhancing the catalytic performance [18, 19]. Bonding interactions between active metal and oxide support depend on the chemical nature and surface properties of support and the electronic structure of metal [18]. The role of the oxide support is not only limited to control the active metal dispersion but also often it has an important influence in the catalytic reaction *via* metal-support interaction [20]. The support can play

a key role in controlling the size, shape, dispersion and structural stability of metal active sites during the reaction. The metal-support interaction can be optimized during the synthesis of the catalyst [21] and the preparation method that provides the opimal metal-interaction interaction is always pursued [22]. For instance, Guil-López et al. [23] demonstrated that Ni–Mg–Al interactions governs the reforming activity and they found that Ni-support interactions depend on the nature of the support and the method of preparation. Özdemir et al. [24] evaluated the effect of the calcination temperature on structural and catalytic properties of $Ni/MgAl_2O_4$ catalyst. They claimed that high calcination temperatures are beneficial to obtain an optimal catalyst which possess strong metal-support interaction, preserves the Ni dispersion high after reduction, increases the surface basicity and stabilizes the Ni particles against sintering.

Within this perspective, a close attention must be played to the preparation method and the treatment stages of the catalyst to achieve an optimal metal support-interaction. Considering all these observations, we have performed a comprehensive study to gain more experimental evidences about how affect the preparation method in the metal-support interaction of Ni-Mg-Al based catalysts for the generation of hydrogen towards methane steam reforming. The control of the oxide-metal interactions provides a unique opportunity to achieve the rational design of catalysts.

2. Experimental

2.1. Catalysts preparation

The catalysts used in this study were prepared using three different procedures, namely (i) impregnation, (ii) coprecipitation-impregnation, and (iii) coprecipitation. The detailed preparation methods of the three catalysts are described below. In all three cases, Al_2O_3/MgO molar ratio of 1 was used to obtain the stoichiometric spinel $MgAl_2O_4$ with nickel loading of 10 wt. %.

(i) For impregnation method, a commercial γ-alumina (Spheralite SCS505) was previously milled to obtain particles below the 100 μm. Then, the alumina was impregnated with a 0.7 M solution of $Mg(NO_3)_2 \cdot 6H_2O$ in ethanol and rotavapored at 50 ºC for removing the solvent excess. Afterwards, the solid was dried overnight at 100 ºC and calcined at 900 ºC for 24 h. The sample was denoted as MgAl (IM). Subsequently, an aqueous 0.05 M solution of nickel precursor salt ($Ni(NO_3)_2 \cdot 6H_2O$) was impregnated on MgAl (IM) and the excess of solvent was removed through roto-evaporation at 50 ºC. Finally, the solid was dried overnight at 100 ºC and calcined at 550 ºC for 4 h. The catalyst obtained using this procedure was labelled Ni-MgAl (IM).

(ii) In the coprecipitation-impregnation method, the support was firstly prepared by coprecipitation of Mg and Al precursor salts and subsequently the nickel was added by impregnation. For it, an aqueous 0.35 M solution of $Mg(NO_3)_2 \cdot 6H_2O$ and 0.7 M of $Al(NO_3)_3 \cdot 9H_2O$ was prepared using an Mg/Al molar ratio of 0.5. An aqueous 2 M solution of NaOH and 0.5 M of Na_2CO_3 was dropped into the above mixture stirring at 70 ºC until pH = 9. The solution obtained was aged in those conditions for 18 h. Once this stage was completed, the sample was filtered and washed with abundant deionized water to remove sodium and carbonate residues. Finally, it was dried overnight at 100 ºC and calcined at 900 ºC for 24 h. The resulting solid was further impregnated with nickel and thermally treated following an identical procedure as the one described above. This support and catalyst were designated as MgAl (CO-IM) and Ni-MgAl (CO-IM), respectively.

(iii) In the other procedure, the catalyst was prepared in a single step by coprecipitation of Ni, Mg and Al. An aqueous solution of the three precursor salts in the form of nitrates $Mg(NO_3)_2 \cdot 6H_2O$ (0.35 M), $Al(NO_3)_3 \cdot 9H_2O$ (0.7 M) and $Ni(NO_3)_2 \cdot 6H_2O$) (0.05 M) was dropped with an aqueous 2 M solution of NaOH and 0.5 M of Na_2CO_3 stirring at 70 ºC until pH = 9 was obtained. The resulting mixture was further aged for 18 h at 70 ºC in agitation. Afterwards, the solid obtained was filtered and washed several times with deionized water to remove sodium and carbonate impurities. Finally, the solid was dried

overnight at 100 ºC and calcined at 550 ºC for 4 h. This catalyst was assigned as Ni-MgAl (CO).

2.2. Characterization techniques

The chemical composition of the solids was estimated by X-ray fluorescence (XRF) spectrometry using a Panalytical AXIOS PW4400 sequential spectrometer with Rh tube as source of radiation. For the measurements, the samples were pelletized onto pressed wafers containing 6 wt. % of wax.

The textural properties of the samples were obtained from nitrogen adsorption-desorption isotherms at liquid nitrogen temperature in a Micromeritics Tristar II apparatus. Before analysis, the samples were degassed at 250 °C for 4 h in vacuum.

The crystalline structure and phases identification of the samples was determined by X-ray diffraction (XRD) on a Siemens D-500 diffractometer equipped with Ni-filtered Cu Kα radiation using a voltage of 40 kV and current of 40 mA. The diffraction patterns were recorded from 10° to 90° (2 theta) in step-scan mode at a step of 0.05° and a counting time of 300 s per step. The crystal structure refinements were performed by means of the Rietveld method using the FULLPROF program [25]. A Thompson–Cox–Hastings pseudo-Voigt function convoluted with an axial divergence asymmetry function was chosen to generate the peak shapes. The following parameters were refined: background points, zero point, scale factor, pseudo-Voigt parameters of the peak shape, atomic positions and cell parameters.

Structural analysis by Raman spectroscopy was performed in a dispersive Horiva Jobin Yvon LabRam HR800 Confocal Raman microscope with a 20 mW He-Ne green laser (532.14 nm) operating at 5 mW and using a grating of 600 grooves mm^{-1}. A 50x objective (Olympus) was used for both focusing the excitation beam on the sample and collecting the scattered light with a confocal pinhole of 1000 μm. The Raman spectrometer was calibrated using a silicon wafer.

Temperature programmed reduction (H_2-TPR) measurements were performed in a conventional U-shaped reactor charged with 50 mg of sample. The temperature was increased from RT to 900 °C with constant heating rate of 10 °C min^{-1} and passing through the catalyst a flow of 50 mL min^{-1} STP certified 5% H_2 in Ar gas mixture. A cold trap of dry ice and acetone was used to condense the water and CO_2 formed during reduction. The H_2 consumption was followed by a TCD detector and quantified by using CuO powder (99.999%) as standard.

Furthermore, the reducibility of the catalysts was also investigated by *in situ* XRD analysis using a high temperature cell Anton Paar HTK 1200 coupled with an X'Pert Pro Philips diffractometer. The system was equipped with X'Celerator detector with a step of 0.05° and a counting time of 300 s per step. The diffractograms were recorded in the 25 – 900 °C temperature range with acquisition per 100 ºC with heating rate of 10 ºC min^{-1} under a flow of 100 mL min^{-1} of 5% H_2 in Ar.

High resolution transmission electron microscopy (HR-TEM) micrographs of the reduced catalysts were obtained on a FEI Talos electron microscope operated at 200 kV and equipped with a field emission filament. For samples preparation, a few milligrams of each catalyst were deposited directly on 300 meshes holey carbon coated copper free TEM-grid. The particle size distribution and the mean particle sizes were estimated from HR-TEM micrographs by single particle measurement of at least 100 particles. The average nickel particle size was estimated using the following equation:

$$D[3,2] = \frac{\sum D_i^3 v_i}{\sum D_i^2 v_i} \quad \text{(Eq. 1)}$$

where *D* is the diameter of the particle and *v* corresponds to the number of particles with this diameter [26].

Temperature-programmed surface reaction of methane (CH_4-TPSR) was carried out in a fixed-bed quartz reactor. The calcined samples were heated from room temperature to 900 ºC under flow of 50 mL min^{-1} STP of 10% v/v CH_4 in Ar. The effluent was monitored

with a mass spectrometer PFEIFFER Vacuum PrismaPlus controlled by Quadera software. The experiments were performed without a previous reduction pretreatment of the sample to investigate the redox abilities of Ni as function of the metal-support interaction. The MS data selected to analyse the evolution of methane decomposition were CH_4 (*m/z* = 15), H_2 (*m/z* = 2), CO (*m/z* = 28) and H_2O (*m/z* = 18) for the Ni catalysts.

Temperature programmed oxidation (TPO) of spent catalysts was conducted in a fixed-bed quartz reactor. The samples were heated from room temperature to 900 ºC with heating rate of 10 °C min^{-1} under a flow of 50 mL min^{-1} STP of 20% v/v O_2 in helium. The CO_2 signal (*m/z* = 44) was followed by mass spectrometry.

2.3. Catalytic activity measurements

Methane steam reforming reaction was carried out in a homemade reaction system including a fixed-bed quartz reactor with internal diameter of 9 mm. The catalytic activity was measured using 100 mg of catalyst diluted in SiC both sieved in the 100-200 µm fractions and achieving a catalytic bed volume of 0.5 mL. Before the reaction, the catalysts were reduced in a flow of 50% H_2/N_2 (100 mL min^{-1} STP) at 800 ºC for 1 h. All reactions were performed at atmospheric pressure in the 750 - 850 ºC temperature range using a steam-to-carbon molar ratio of 1.24 (27.7 mL min^{-1} STP of H_2O and 23.3 mL min^{-1} STP of CH_4), and a space velocity of 60 L g^{-1} h^{-1}. Reactants and products were analysed and quantified by gas chromatography using an Agilent 7890A model gas chromatograph equipped with a Porapak® Q, a Molecular Sieve 5A, and two thermal conductivity detectors (TCD). The CH_4 conversion and H_2 yield was calculated according to Eqs. (2) and (3), respectively:

$$\mathrm{CH_4\ conversion\ (\%)} = \frac{n_{CH4in} - n_{CH4out}}{n_{CH4in}} \mathrm{x100} \qquad \text{(Eq. 2)}$$

$$\mathrm{H_2\ yield\ (\%)} = \frac{n_{H2out}}{2\,n_{CH4in} + n_{H2Oin}} \mathrm{x100} \qquad \text{(Eq. 3)}$$

Being *n* the molar flow of CH_4, H_2O and H_2 respectively and the subscripts *in* or *out* correspond to the inlet or the outlet flow.

3. Results and discussion

3.1. Chemical composition and textural properties

Chemical compositions obtained by XRF (Table 1) indicate that the loading of Ni, Mg and Al were almost identical to the nominal values for both Ni-MgAl (IM) and Ni-MgAl (CO-IM) catalysts. This indicates that these preparation methods were carried out effectively in both cases. Nevertheless, the Ni-MgAl (CO) catalyst presents a higher value of Ni content than the theoretical one. This fact is owed to the amphoteric nature of Mg $(OH)_2$, which has a K_{sp} of 5.61 x 10^{-12} much higher than $Ni(OH)_2$ (5.48 x 10^{-16}) and $Al(OH)_3$ (3 x 10^{-32}). Consequently, the partial precipitation of Mg provokes a small loss of Mg^{2+} increasing the Ni content [27]. The Al content also was below the nominal value in this latter sample, which can be related with a small loss of Al ions during the coprecipitation and the washing steps.

The textural properties of the supports and catalysts prepared are also listed in Table 1. It can be noticed that the support prepared by impregnation method leads to lower specific surface area (S_{BET}) compared to the support prepared by coprecipitation method. This observation indicates that the preparation method affects directly to the textural properties of the $MgAl_2O_4$ spinel. On the other hand, a slight decrease in the specific surface area and pore volume was observed in both supports after Ni impregnation, indicating that nickel species were incorporated inside the pores of the support. Regarding the Ni-MgAl (CO) catalyst, this sample showed the smaller average pore diameter. However, the value of specific surface measured for this sample is similar to the value obtained for Ni-MgAl (CO-IM) sample.

Figure 1 shows the nitrogen adsorption-desorption isotherms and pore size distributions for all the prepared samples after calcination. As can be observed, the isotherms of all

the solids were type IV, suggesting the formation of a mesoporous structure according to the IUPAC classification. However, notably differences can be appreciated in the hysteresis loop. The MgAl (IM) and Ni-MgAl (IM) sample have a typical H3 hysteresis loop closing at p/p_0 lower than 0.4 that can be associated to non-uniform interparticle pores while that the MgAl (CO-IM), Ni-MgAl (CO-IM) and Ni-MgAl (CO) samples have a H1 hysteresis loop which corresponds to agglomerated particles with uniform pore size. These isotherms are corroborated by the pore diameter distribution included in Figure 1b. The Ni-MgAl (CO), MgAl (CO-IM) and Ni-MgAl (CO-IM) samples present a narrow pore size distribution while the MgAl (IM) and Ni-MgAl (IM) solids have a broader pore size distribution. The presence of smaller mesopores in the Ni-MgAl (CO) catalyst could be attributed to the incorporation of Ni and Mg into the structure modifying the porosity of the material and decreasing the pore size [28].

3.2. Structural analysis

Powder X-ray diffraction was used to identify the crystalline phases existing in the prepared samples. In order to deepen the structural study, a Rietveld refinement analysis was performed on the prepared samples. In figure 2 are depicted the experimental and the calculated XRD profiles for all the prepared samples. As can be observed, MgAl (IM) and MgAl (CO-IM) supports are formed essentially by the stoichiometric spinel $MgAl_2O_4$ together with small aggregates of MgO. However, it should be noted that the amount of MgO decreases in the MgAl (CO-IM) support whereas a non-stoichiometric spinel $(Mg_{0.4}Al_{0.6})Al_{1.8}O_4$ is formed. This preferential formation of spinel against the MgO phase observed in the latter support can be explained assuming the intimal contact that takes place between the Mg^{2+} and Al^{3+} ions during the coprecipitation method. After impregnation of nickel and subsequent calcination, it is clearly observed for both Ni-MgAl (IM) and Ni-MgAl (CO-IM) catalysts that nickel species appear mainly as NiO although a small portion of nickel ions are incorporated in the $MgAl_2O_4$ forming non-stoichiometric mixed oxides in both cases. Noteworthy that the signals of NiO could be masked by the

presence of MgO phase. Nevertheless, we can assume that the formation of $MgAl_2O_4$ spinel and NiO takes place preferentially with respect to the formation of MgO and/or $NiAl_2O_4$ phase at the temperature at which the catalysts were calcined (550 ºC). This assumption is in agreement with the previous work of Jacob and Alcok [29], who studied the formation of $NiAl_2O_4$-$MgAl_2O_4$ spinel solids solutions. Moreover, it can be noticed that MgO and the non-stoichiometric spinel $(Mg_{0.4}Al_{0.6})Al_{1.8}O_4$ are absent in the Ni-MgAl (CO-IM) catalyst. This might be because of a part of Ni is forming the rock-salt type Mg-Ni-O solid solution in the mixed oxide [30], and another part of Ni is occupying the octahedral sites of the non-stoichiometric Mg-Al spinel. Therefore, it would be expected that the interaction Ni-support were strong in this case resulting a better dispersion of Ni metal particles after reduction as will be discussed later in the next subsection. Concerning the Ni-MgAl (CO) catalyst, it can be observed the presence of two types of solid solution, $(Ni\text{-}Mg)_{1-x}Al_{2-y}O_{4-x-1.5y}$ and (Mg-Ni)O. As shown figure 2, the peaks ascribed to the (Mg-Ni)O solid solution in this sample are very broad suggesting that this solution become amorphous or the crystal size is very small. The results obtained are summarized in Table 2. The goodness of fit, χ^2, show that the optimal fitting was attained in this Rietveld analysis [31].

Raman spectra of the calcined catalysts are displayed in Figure 3. The $MgAl_2O_4$ spinel has a cubic close-packed structure whose spatial group is Fd-3m. Group theory predicts that the active vibrational modes in Raman are $A_{1g}+E_g+3T_{2g}$ [32]. This technique does not allow discriminating between the $NiAl_2O_4$ and $MgAl_2O_4$ spinels in the samples because they have identical structure and the spectra recorded are analogous. However, the formation of a mixed $NiMgAl_2O_4$ spinel involves a distortion in the crystalline lattice due to the insertion of Ni^{2+} in the octahedral sites not occupied by Mg^{2+} in the $MgAl_2O_4$ spinel.

The bands observed at 311, 407, 680 and 767 cm^{-1} are assigned to the vibrational modes $T_{2g}^{(1)}$, E_g, $T_{2g}^{(2)}$ and A_{1g}, respectively, of spinel-like structure [33]. These features were

observed in the three catalysts. Additionally, it appears a broad band at 560 cm^{-1} with a shoulder at 485 cm^{-1} and another band at 1063 cm^{-1}. The bands at 560 cm^{-1} and 485 cm^{-1} are attributed to the first-order longitudinal optical (LO) and transverse optical (TO) one-phonon modes, respectively [34], whereas the band at 1063 cm^{-1} is ascribed to the two-phonons modes (2LO), all of them characteristic of NiO [35, 36]. It should be noticed that in the Ni-MgAl (CO) catalyst the band at 1063 cm^{-1} was more intense and sharper than in the other two catalysts. This fact could be associated with the lower degree of interaction between the NiO phase and the support, and thus the presence of bigger crystallites of NiO on the surface [35, 37].

3.3. Reducibility of the catalysts

The reducibility of the nickel species in the three prepared catalysts was investigated by hydrogen temperature-programmed reduction measurements (H_2-TPR), and the results obtained are depicted in Figure 4. All the catalysts showed a reduction process in the temperature range between 300 - 750 ºC that can be attributed to the reduction of NiO species with different degree of interaction with the support [15]. Additionally, one second reduction peak in the 750 - 900 ºC temperature range was observed on the Ni-MgAl (IM) and Ni-MgAl (CO-IM) catalysts that likely is related to the reduction of $NiAl_2O_4$ species which are strongly interacting with the support [38]. The interaction strength between the nickel particles and the support influences notably in the reduction profiles and typically the reduction of NiO species are shifted to higher temperatures for strong metal-support interactions while the reduction of NiO at lower temperatures can be associated with weak interactions and/or bigger metal particles [39]. From TPR profiles observed in Fig.4 can be deduced that the interaction between nickel species and support decreases in the order Ni-MgAl (IM) ≥ Ni-MgAl (CO-IM) > Ni-MgAl (CO).

The degree of reducibility of the catalysts was estimated from the area under the TPR profile assuming that the only reducible species are Ni^{2+}, which is reduced to metallic nickel species. As shown Table 1, the nickel was totally reduced in the Ni-MgAl (CO)

sample while in the other two catalysts only a similar percentage of ca. 65-70 % of nickel species were reduced. This reveals that at least a part of nickel is not being reduced in the latter catalysts probably due to the presence of the $NiAl_2O_4$ spinel or the strong interaction NiO – $MgAl_2O_4$ in good agreement with the XRD results. Although the amount of reducible nickel species in Ni-MgAl (IM) and Ni-MgAl (CO-IM) catalysts are very similar, the reduction temperature for Ni-MgAl (IM) is higher for Ni-MgAl (CO-IM). This suggests that a strong interaction of metal with the support could difficult the reduction of the nickel species in the Ni-MgAl (IM) catalyst decreasing thus the number of nickel active species for methane steam reforming.

In situ XRD reduction measurements were carried out to investigate the structural modifications during the reduction pretreatment. As shown in Figure 5a, it can be noticed the appearance of three new diffraction peaks at 44º, 51º and 62º at temperatures above 600 ºC that evidences the formation of metallic nickel (JDPDS 00-004-0850) during the reduction treatment in all the cases. It is remarkable the fact that in the Ni-MgAl (CO) catalyst these three peaks become very sharp and intense as the temperature increases whereas in the other two catalysts those lines are wider. The average crystallite size of Ni^0 was calculated using the Scherrer equation from the line widths of the XRD peaks corresponding to (200) crystal plane (peak at 51º). Figure 5b included the estimated values of crystallite size of Ni^0 as function of the reduction temperature. It can be noted that the growth of Ni^0 crystallites during reduction is lower for Ni-MgAl (CO-IM) and Ni-MgAl (IM) catalysts. However, the reduction at high temperatures in the Ni-MgAl (CO) catalyst produces an agglomeration of the nickel on surface producing the sintering of metal. This latter observation suggests a weaker interaction between the nickel and the support in the Ni-MgAl (CO) sample in comparison with the other two catalysts, Ni-MgAl (IM) and Ni-MgAl (CO-IM), which present a stronger Ni-support interaction and the sintering of nickel particles is minimised. The growth of metallic nickel particles during the reduction process depends on the interaction strength between nickel species and

the support [39] and these results are in good agreement with the above mentioned TPR profiles.

Regarding the results of H_2-TPR and *in situ* XRD, it can be deduced that the reducibility of the catalysts depends notably on the metal-support interaction. A strong interaction prevents the nickel sintering although can affect negatively avoiding the reduction of nickel species and thus decreasing the number of nickel active sites.

Furthermore, the reduced catalysts were studied by HR-TEM in order to compare the particles size distribution with the crystallite size of metallic Ni estimated by Scherrer equation from *in situ* XRD data. The representative micrographs and nickel particle sizes distribution of the reduced samples are shown in Figure 6. As can be noticed, the mean particles sizes estimated after reductions are in concordance with the *in situ* XRD observation previously discussed. There is a major agglomeration of Ni particles on Ni-MgAl (CO) catalyst whereas the Ni-MgAl (CO-IM) sample is composed by smaller particles and more homogeneous particles distribution. Thus, the metal-support interaction is affected by the preparation method of the sample.

3.3. Temperature-programmed surface reaction with methane (CH_4-TPSR)

CH_4-TPSR measurements were carried out to study the evolution of species resulting from the interaction of methane with catalyst surface in all calcined catalysts (Figure 7). Comparing the CH_4-TPSR profiles in Fig. 7, it can be noted a significant loss of water of the solids between 100 and 450 ºC in the Ni-MgAl (CO) catalyst. This indicates the presence of a large amount of structural water and surface hydroxides species in this catalyst that could be due to the low calcination temperature (550 ºC). By contrast, both supports of Ni-impregnated catalysts (Ni-MgAl (IM) and Ni-MgAl (CO-IM)) were calcined at 900 ºC and these samples only showed a weak peak of desorption of water at temperatures below 200 ºC that corresponds basically to physisorbed water. The high calcination temperature increases the crystallinity of the samples and eliminates the

occluded water in the structure. As shown in Fig. 7, it can be seen that the preparation method influences notably the methane decomposition reaction. Methane decomposition over the three Ni catalysts starts at temperatures higher than 450 ºC and it is observed a broad consumption peak of methane that is accompanied by the production of CO and H_2. It should be noted that in the Ni-MgAl (CO) catalyst occurs an important reduction of the methane decomposition rate in the 650 – 750 ºC temperature range and from this temperature methane is probably decomposed by thermal reactions. This observation agrees with *in situ* XRD results in which sintering of Ni particles was observed above 750 ºC. On the other two catalysts, one can see different methane decomposition peaks as function of the temperature that are related with the strength of interaction between the Ni and the support in agreement with the reducibility results.

It is well known that the decomposition of methane into CH_x fragments depend strongly on the Ni particles and their interaction with the support [40]. Dehydrogenation of methane is highly active in active defect sites and the decomposition rate increase with decreasing the particle size [41]. Methane decomposition over nickel oxides occurs towards the following elementary reaction steps [42]:

$$CH_4\,(g) \rightarrow H^* + CH_3^* \quad (3)$$

$$CH_3^* \rightarrow H^* + CH_2^* \quad (4)$$

$$CH_2^* \rightarrow H^* + CH^* \quad (5)$$

$$CH^* \rightarrow H^* + C(s) \quad (6)$$

$$C\,(s) + O^* \rightarrow CO\,(g) \quad (7)$$

Methane is decomposed into CH_x fragments (reactions 3 - 6) over NiO sites producing H_2 (g) and carbon deposits. Subsequently, the carbon species generated are oxidized by the lattice oxygen forming CO (g) and metallic nickel (reaction 7). This sequence of

reactions explains the presence of CO observed during the methane reaction decomposition in the three samples.

3.4. Activity tests for methane steam reforming

Figure 8 includes the methane conversion and the hydrogen yield as function of the reaction temperature obtained for the three Ni catalysts prepared by the different methods. As can be observed, both conversion and yield increased with the temperature in all the samples and followed an order of Ni-MgAl (CO-IM) > Ni-MgAl (IM) > Ni-MgAl (CO). Interestingly, Ni-MgAl (CO-IM) catalyst exhibited the highest methane conversion and hydrogen yield. This may be due to the fact that in this catalyst there are a considerable amount of metallic Ni small particles highly actives and well dispersed on the $MgAl_2O_4$ support. By contrast, the results of TPR (Fig.4) showed that in the Ni-MgAl (IM) catalyst Ni species have strong interactions with the support ($MgAl_2O_4$) or is forming part of the structure $NiMgAl_2O_4$, being thus hardly reducible and consequently less active. On the other hand, the low activity observed in Ni-MgAl (CO) catalyst can be attributed to the presence of large Ni particles formed during the reduction pretreatment that decreases notably the effectivity of the catalyst. Numerous studies have demonstrated that the catalytic activity for methane steam reforming is affected by the nickel particle size, metal dispersion and the interaction of the nickel particles with the support [43, 44].

For better comparison, we have estimated the intrinsic site activity of the three catalysts in order to evaluate the relative efficiency of the Ni sites. The intrinsic activity provides direct information about the catalytic essence correlating the nature with the structure of the active sites. The parameter used for this purpose was the turnover frequency (TOF), which represents the number of molecules of methane transformed per active site and per second according to the following equation (Eq. 4):

$$\mathrm{TOF} = \frac{\mathrm{r}}{\mathrm{D_{Ni}}}\,[\mathrm{s}^{-1}] \qquad \text{(Eq. 4)}$$

where *r* is the reaction rate expressed as moles of CH_4 transformed per mol of Ni and per second, and D_{Ni} corresponds to the nickel dispersion [45]. The nickel dispersion was determined on the basis of a cuboctahedron shape model assuming the average Ni particle size obtained by TEM (Figure 6) for the reduced catalysts [46]. The dispersion discloses the total number of nickel atoms accessible for the steam reforming of methane reaction. The estimated values of Ni dispersion after reduction at 800 ºC are included in Table 1. As can be observed, the three Ni-based catalysts presented a similar value of Ni dispersion. From Figure 9, it can be seen that the Ni-MgAl (CO) exhibits a poor catalytic activity in the methane steam reforming reaction while Ni-MgAl (CO-IM) sample presents the highest specific reaction rate. The obtained catalytic data correlate with the balance between the strength of the metal-support interaction and the reducibility of the catalyst. The catalytic performance can be increased by boosting the number of active nickel sites on the surface of reduced catalysts. Among the catalysts tested, Ni-MgAl (CO-IM) catalyst has the optimal metal-support interaction exhibiting the best catalytic performance in terms of methane conversion and hydrogen production. Therefore, it can be assumed that the catalytic activity can be improved by controlling the balance between the reduction degree and the strength of the metal-support interaction towards the adequate preparation method. These results are in agreement with the data reported by Nieva et al. [47] in which large Ni particles with none metal-support interaction led to a very unstable and inactive catalysts whereas small Ni particles in intimate contact with a zinc or magnesium aluminate-like matrix are catalysts highly active in steam reforming of methane.

3.5. Study of carbon deposits

Temperature-programmed oxidation (TPO) analysis and Raman spectroscopy were used to characterize the coke species deposited on the three catalysts after methane steam reforming reaction. Figure 10 displays the evolution of the *m/z* = 44 signals assigned to CO_2 during the TPO experiments for the three spent catalysts. From a

quantitative point of view, as the area under the TPO curve is proportional to the amount of deposited carbon, it can be stated that the carbon deposited in the Ni-MgAl (CO) catalyst is relatively smaller in comparison with the other two catalysts. The temperature at which the CO_2 maximum appeared provides information about the nature of the carbonaceous species deposited onto the catalyst surface. These carbonaceous deposits have different structure orders and morphologies depending on the reaction conditions and the structure of the catalyst. Zhang and Verykios [48] classified the coke deposits in three types, designed as C_α, C_β and C_γ, respectively. The assigned to C_α usually corresponds to amorphous carbon and can be removed at low temperatures whereas C_β and C_γ are associated to graphitic or filamentous carbon species very thermally stable. These latter carbon species are hardly gasified and consequently are causing of the catalyst deactivation. The TPO results displayed in Figure 10 show that the amount of C_β and C_γ carbon species are considerably larger in the two impregnated catalysts. This fact can be understood taking into account that the specific activity for methane transformation is significantly minor in the Ni-MgAl (CO) catalyst in comparison with the other two Ni-impregnated catalysts. Another aspect to be considered is the acid-base properties of the samples. Ni-MgO (CO) sample is essentially composed by a NiO-MgO solid solution and it is well known that MgO is the responsible for the alkaline character. The presence of MgO favors the gasification of carbonaceous deposits [49]. In contrast, for Ni-impregnated catalysts, the nickel species are supported and dispersed on $MgAl_2O_4$ spinels. The absence or low content of MgO on surface could increase the acidity in the sample promoting an increase of the amount of coke deposited.

The nature of carbon deposits was also evaluated by Raman spectroscopy. As can be observed in Fig. 11, the spectra obtained for all spent catalysts showed two characteristic bands, one at 1348 cm^{-1} (D-band) associated to the morphological disorder and defects corresponding to graphite with structural imperfections and/or amorphous carbon, and another one at 1589 cm^{-1} (G-band) that is ascribed to the in-plane C-C stretching

vibrations characteristic of ordered structure carbon [50]. Moreover, it should be noticed the appearance of a weak shoulder at ca. 1620 cm^{-1} (D´-band) and although its connotation is not well understood it is believed that is related to the presence of defects in the graphite structure [51]. In order to identify the structural differences between the carbon species deposited on the samples, Beyssac et al. [52] proposed a simple classification according to the value of R2, which is estimated from the D-to-(G+D) bands intensity ratio. These authors suggested that values of R2 higher than 0.5 are typical of amorphous carbon species while that values lower than 0.5 correspond to structural carbon species. As shown Fig. 11, the Ni-MgAl (IM) and Ni-MgAl (CO-IM) catalysts presented values of R2 slightly lower than 0.5 whereas the Ni-MgAl (CO) sample shows a value of R2 superior to 0.5. This observation indicates that the carbon deposited on the latter catalyst is more amorphous in agreement with the TPO results.

Considering findings mentioned above in combination with the economic feasibility of Ni-based catalysts, it can be concluded that in view of designing a commercial catalyst for steam reforming, it is crucial the utilization of an adequate preparation method, to adjust the metal-support interaction and the reducibility of the active metal.

4. Conclusions

The degree of nickel-support interaction plays a fundamental role in the performance of nickel-based catalysts. The goal of the present study was to investigate the influence of the preparation method on the degree of Ni-Mg-Al interaction and the structure-activity relationship in the methane steam reforming reaction. Differences observed in activity are related to the degree of Ni-Mg-Al interaction and according to the reducibility results the Ni-MgAl (CO-IM) catalyst presented the optimal metal-support interaction to reduce the NiO at lower temperatures and preserve the Ni^0 particles highly dispersed on the support surface. This catalyst is basically formed of very small Ni particles strongly interacting with the $MgAl_2O_4$ spinel-like matrix and exhibits the higher catalytic activity and the major production of hydrogen. In conclusion, these results demonstrate that the

structure and catalytic performance of Ni based catalysts can be tuned by controlling the Ni-support interaction towards of the preparation method.

Acknowledgments

Financial support for this work has been obtained from the Spanish Ministerio de Economía y Competitividad – MINECO (ENE2015-66975-C3-2-R) co-financed by FEDER funds from the European Union. Lola Azancot and José L. Santos acknowledge the MINECO for their PhD fellowship BES-2016-0077475 and BES-2014-068244, respectively. Moreover, Luis F. Bobadilla and José M. Córdoba thank the contracts of Spanish Government financed in part by the European Regional Development Fund through the “Juan de la Cierva incorporación” program (IJCI-2015-26348) and “Ramón y Cajal” program (RYC-2013-12437), respectively.

References

[1] S. Sengodan, R. Lan, J. Humphreys, D. Du, W. Xu, H. Wang, S. Tao, Advances in reforming and partial oxidation of hydrocarbons for hydrogen production and fuel cell applications, Renew. Sustain. Energy Rev., 82 (2018) 761-780.

[2] J.R. Rostrup-Nielsen, Conversion of hydrocarbons and alcohols for fuel cells, Phys. Chem. Chem. Phys., 3 (2001) 283-288.

[3] S.D. Angeli, G. Monteleone, A. Giaconia, A.A. Lemonidou, State-of-the-art catalysts for CH_4 steam reforming at low temperature, Int. J. Hydrogen Energy, 39 (2014) 1979-1997.

[4] A. Ricca, V. Palma, M. Martino, E. Meloni, Innovative catalyst design for methane steam reforming intensification, Fuel, 198 (2017) 175-182.

[5] K.Y. Koo, H.-S. Roh, U.H. Jung, D.J. Seo, Y.-S. Seo, W.L. Yoon, Combined H_2O and CO_2 reforming of CH_4 over nano-sized Ni/MgO-Al_2O_3 catalysts for synthesis gas production for gas to liquid (GTL): Effect of Mg/Al mixed ratio on coke formation, Catal. Today, 146 (2009) 166-171.

[6] K.Y. Koo, J.H. Lee, U.H. Jung, S.H. Kim, W.L. Yoon, Combined H_2O and CO_2 reforming of coke oven gas over Ca-promoted Ni/$MgAl_2O_4$ catalyst for direct reduced iron production, Fuel, 153 (2015) 303-309.

[7] J.R. Rostrup-Nielsen, Catalytic Steam Reforming, in: J.R. Anderson, M. Boudart (Eds.) Catalysis: Science and Technology, Springer Berlin Heidelberg, Berlin, Heidelberg, 1984, pp. 1-117.

[8] J. Guo, H. Lou, H. Zhao, D. Chai, X. Zheng, Dry reforming of methane over nickel catalysts supported on magnesium aluminate spinels, Appl. Catal. A Gen., 273 (2004) 75-82.

[9] L.J.I. Coleman, W. Epling, R.R. Hudgins, E. Croiset, Ni/Mg–Al mixed oxide catalyst for the steam reforming of ethanol, Appl. Catal. A Gen., 363 (2009) 52-63.

[10] C. García-Sancho, R. Guil-López, A. Sebastián-López, R.M. Navarro, J.L.G. Fierro, Hydrogen production by methane decomposition: A comparative study of supported and bulk ex-hydrotalcite mixed oxide catalysts with Ni, Mg and Al, Int. J. Hydrogen Energy, 43 (2018) 9607-9621.

[11] A. Djaidja, H. Messaoudi, D. Kaddeche, A. Barama, Study of Ni–M/MgO and Ni–M–Mg/Al (M=Fe or Cu) catalysts in the CH_4–CO_2 and CH_4–H_2O reforming, Int. J. Hydrogen Energy, 40 (2015) 4989-4995.

[12] A. Djaidja, A. Kiennemann, A. Barama, Effect of Fe or Cu addition on Ni/Mg-Al and Ni/MgO catalysts in the steam-reforming of methane, in: E.M. Gaigneaux, M. Devillers, D.E. De Vos, S. Hermans, P.A. Jacobs, J.A. Martens, P. Ruiz (Eds.) Stud. Surf. Sci. Catal., Elsevier, 2006, pp. 945-952.

[13] D. Li, T. Shishido, Y. Oumi, T. Sano, K. Takehira, Self-activation and self-regenerative activity of trace Rh-doped Ni/Mg(Al)O catalysts in steam reforming of methane, Appl. Catal. A Gen., 332 (2007) 98-109.

[14] X. Lin, R. Li, M. Lu, C. Chen, D. Li, Y. Zhan, L. Jiang, Carbon dioxide reforming of methane over Ni catalysts prepared from Ni–Mg–Al layered double hydroxides: Influence of Ni loadings, Fuel, 162 (2015) 271-280.

[15] O.W. Pérez-López, A. Senger, N.R. Marcilio, M.A. Lansarin, Effect of composition and thermal pretreatment on properties of Ni–Mg–Al catalysts for CO_2 reforming of methane, Appl. Catal. A Gen., 303 (2006) 234-244.

[16] D. Li, L. Wang, M. Koike, Y. Nakagawa, K. Tomishige, Steam reforming of tar from pyrolysis of biomass over Ni/Mg/Al catalysts prepared from hydrotalcite-like precursors, Appl. Catal. B Environ., 102 (2011) 528-538.

[17] S. Katheria, A. Gupta, G. Deo, D. Kunzru, Effect of calcination temperature on stability and activity of Ni/$MgAl_2O_4$ catalyst for steam reforming of methane at high pressure condition, Int. J. Hydrogen Energy, 41 (2016) 14123-14132.

[18] S. Najafishirtari, C. Guglieri, S. Marras, A. Scarpellini, R. Brescia, M. Prato, G. Righi, A. Franchini, R. Magri, L. Manna, M. Colombo, Metal-support interaction in catalysis: The influence of the morphology of a nano-oxide domain on catalytic activity, Appl. Catal. B Environ., 237 (2018) 753-762.

[19] M. Ahmadi, H. Mistry, B. Roldan Cuenya, Tailoring the catalytic properties of metal nanoparticles via support interactions, J. Phys. Chem. Lett., 7 (2016) 3519-3533.

[20] R.M. Palomino, R. Hamlyn, Z. Liu, D.C. Grinter, I. Waluyo, J.A. Rodriguez, S.D. Senanayake, Interfaces in heterogeneous catalytic reactions: Ambient pressure XPS as a tool to unravel surface chemistry, J. Electron Spectrosc. Relat. Phenomena, 221 (2017) 28-43.

[21] F. Wang, L. Xu, J. Zhang, Y. Zhao, H. Li, H.X. Li, K. Wu, G.Q. Xu, W. Chen, Tuning the metal-support interaction in catalysts for highly efficient methane dry reforming reaction, Appl. Catal. B Environ., 180 (2016) 511-520.

[22] M. Cargnello, P. Fornasiero, R.J. Gorte, Opportunities for tailoring catalytic properties through metal-support interactions, Catal. Lett., 142 (2012) 1043-1048.

[23] R. Guil-López, R.M. Navarro, A.A. Ismail, S.A. Al-Sayari, J.L.G. Fierro, Influence of Ni environment on the reactivity of Ni–Mg–Al catalysts for the acetone steam reforming reaction, Int. J. Hydrogen Energy, 40 (2015) 5289-5296.

[24] H. Özdemir, M.A.F. Öksüzömer, M.A. Gürkaynak, Effect of the calcination temperature on Ni/$MgAl_2O_4$ catalyst structure and catalytic properties for partial oxidation of methane, Fuel, 116 (2014) 63-70.

[25] R.A. Young, The Rietveld method, Oxford Scientifics Publications, Oxford, 1995.

[26] D. Su, Advanced electron microscopy characterization of nanomaterials for catalysis, Green Energy Environ., 2 (2017) 70-83.

[27] J. Huang, W. Liu, Y. Yang, Phase interactions in Mg-Ni-Al-O oxygen carriers for chemical looping applications, Chem. Eng. J., 326 (2017) 470-476.

[28] H. Arbag, Effect of impregnation sequence of Mg on performance of mesoporous alumina supported Ni catalyst in dry reforming of methane, Int. J. Hydrogen Energy, 43 (2018) 6561-6574.

[29] K.T. Jacob, C.B. Alcock, Activities and their relation to cation distribution in $NiAl_2O_4$-$MgAl_2O_4$ spinel solid solutions, J. Solid State Chem., 20 (1977) 79-88.

[30] K. Takehira, T. Shishido, P. Wang, T. Kosaka, K. Takaki, Steam reforming of CH_4 over supported Ni catalysts prepared from a Mg–Al hydrotalcite-like anionic clay, Phys. Chem. Chem. Phys., 5 (2003) 3801-3810.

[31] J.M. Córdoba, M. Ponce, M.J. Sayagués, Structure evolution in the $LaMn_{1-x}Fe_xO_{3+\delta}$ system by Rietveld analysis, Solid State Ion., 303 (2017) 132-137.

[32] N.V. Minh, I.-S. Yang, A Raman study of cation-disorder transition temperature of natural MgAl2O4 spinel, Vib. Spectrosc., 35 (2004) 93-96.

[33] P. Thibaudeau, F. Gervais, Ab initio investigation of phonon modes in the MgAl2O4 spinel, J. Phys.: Condens. Matter 14 (2002) 3543–3552.

[34] A.V. Ghule, K. Ghule, S.-H. Tzing, T.H. Punde, H. Chang, Y.C. Ling, Thermo-Raman spectroscopy in situ monitoring study of solid-state synthesis of NiO–Al_2O_3 nanoparticles and its characterization, J. Solid State Chem., 182 (2009) 3406-3411.

[35] S.K. Yadav, P. Jeevanandam, Synthesis of NiO–Al_2O_3 nanocomposites by sol–gel process and their use as catalyst for the oxidation of styrene, J. Alloys Comp., 610 (2014) 567-574.

[36] R. Benrabaa, A. Barama, H. Boukhlouf, J. Guerrero-Caballero, A. Rubbens, E. Bordes-Richard, A. Löfberg, R.-N. Vannier, Physico-chemical properties and syngas production via dry reforming of methane over $NiAl_2O_4$ catalyst, Int. J. Hydrogen Energy, 42 (2017) 12989-12996.

[37] J. Pérez-Ramirez, G. Mul, J.A. Moulijn, In situ fourier transform infrared and laser Raman spectroscopic study of the thermal decomposition of Co-Al and Ni-Al hydrotalcites, Vib. Spectrosc., 27 (2001) 75-88.

[38] Z. Alipour, M. Rezaei, F. Meshkani, Effect of Ni loadings on the activity and coke formation of MgO-modified Ni/Al_2O_3 nanocatalyst in dry reforming of methane, J. Energy Chem., 23 (2014) 633-638.

[39] A.R. González, Y.J.O. Asencios, E.M. Assaf, J.M. Assaf, Dry reforming of methane on Ni–Mg–Al nano-spheroid oxide catalysts prepared by the sol–gel method from hydrotalcite-like precursors, Appl. Surf. Sci., 280 (2013) 876-887.

[40] J. Guo, H. Lou, X. Zheng, The deposition of coke from methane on a $Ni/MgAl_2O_4$ catalyst, Carbon, 45 (2007) 1314-1321.

[41] H.S. Bengaard, J.K. Nørskov, J. Sehested, B.S. Clausen, L.P. Nielsen, A.M. Molenbroek, J.R. Rostrup-Nielsen, Steam reforming and graphite formation on Ni catalysts, J. Catal., 209 (2002) 365-384.

[42] P.N. Kechagiopoulos, S.D. Angeli, A.A. Lemonidou, Low temperature steam reforming of methane: A combined isotopic and microkinetic study, Appl. Catal. B Environ., 205 (2017) 238-253.

[43] A. Gil, A. Díaz, L.M. Gandía, M. Montes, Influence of the preparation method and the nature of the support on the stability of nickel catalysts, Appl. Catal. A Gen., 109 (1994) 167-179.

[44] J.G. Seo, M.H. Youn, J.C. Jung, I.K. Song, Effect of preparation method of mesoporous $Ni–Al_2O_3$ catalysts on their catalytic activity for hydrogen production by steam reforming of liquefied natural gas (LNG), Int. J.Hydrogen Energy, 34 (2009) 5409-5416.

[45] J.G.G. Jr, S. Kim, W.D. Rhodes, Turnover frequencies in metal catalysis: Meanings, functionalities and relationships, in: J.J. Spivey, G.W. Roberts (Eds.) Catalysis: Volume 17, The Royal Society of Chemistry, 2004, pp. 320-348.

[46] A. Borodziński, M. Bonarowska, Relation between crystallite Size and dispersion on supported metal catalysts, Langmuir, 13 (1997) 5613-5620.

[47] M.A. Nieva, M.M. Villaverde, A. Monzón, T.F. Garetto, A.J. Marchi, Steam-methane reforming at low temperature on nickel-based catalysts, Chem. Eng. J., 235 (2014) 158-166.

[48] Z.L. Zhang, X.E. Verykios, Carbon dioxide reforming of methane to synthesis gas over supported Ni catalysts, Catal. Today, 21 (1994) 589-595.

[49] A. Penkova, L. Bobadilla, S. Ivanova, M.I. Domínguez, F. Romero-Sarria, A.C. Roger, M.A. Centeno, J.A. Odriozola, Hydrogen production by methanol steam reforming on NiSn/MgO–Al_2O_3 catalysts: The role of MgO addition, Appl. Catal. A Gen., 392 (2011) 184-191.

[50] C. Anjaneyulu, G. Naresh, V.V. Kumar, J. Tardio, T.V. Rao, A. Venugopal, Influence of Rare Earth (La, Pr, Nd, Gd, and Sm) Metals on the methane decomposition activity of Ni–Al catalysts, ACS Sustain. Chem. Eng., 3 (2015) 1298-1305.

[51] T. Jawhari, A. Roid, J. Casado, Raman spectroscopic characterization of some commercially available carbon black materials, Carbon, 33 (1995) 1561-1565.

[52] O. Beyssac, B. Goffé, J.-P. Petitet, E. Froigneux, M. Moreau, J.-N. Rouzaud, On the characterization of disordered and heterogeneous carbonaceous materials by Raman spectroscopy, Spectrochim. Acta Part A Mol. Biomol. Spectrosc. 59 (2003) 2267-2276.

LIST OF TABLES AND FIGURES

Table 1. Composition, physicochemical properties and reducibility of the prepared samples.

Sample	Chemical composition (wt.%)			Textural properties			Reducibility degree (%)	Metal Ni dispersion (%)
	MgO	Al_2O_3	Ni	S_{BET} $m^2 g^{-1}$	V_{pore} $cm^3 g^{-1}$	D_{pore} nm		
Ni-MgAl (CO)	42.3 (25)	39.8 (65)	17.9 (10)	64	0.13	6.1	100	7
Ni-MgAl (CO-IM)	23.8 (25)	62.8 (65)	13.4 (10)	71	0.24	10.5	65	8
MgAl (CO-IM)	-	-	-	79	0.3	15.9	-	-
Ni-MgAl (IM)	29.2 (25)	58.5 (65)	12.3 (10)	31	0.14	11.5	70	8
MgAl (IM)	-	-	-	38	0.2	10	-	-

Nominal values of Ni loading wt. % are included between parentheses

Ni dispersion is estimated according to the model proposed by Borodziński et al. [46]

Table 2. Rietveld refinement results for the prepared samples. The values in the table are expressed in wt.% of crystallite phases.

Sample	$MgAl_2O_4$	MgO	NiO	$(Mg_{0.4}Al_{0.6})Al_{1.8}O_4$	Solid solution $(Ni\text{-}Mg)_{1-x}Al_{2-y}O_{4-x-1.5y}$	(Mg-Ni)O	X^2
Ni-MgAl (CO)	-	-	-	-	28	72	9.6
Ni-MgAl (CO-IM)	86.4*	-	13.6	-	-	-	3.4
MgAl (CO-IM)	86	2.3	-	11.7	-	-	8.6
Ni-MgAl (IM)	80.7**	5.5	13.9	-	-	-	4.9
MgAl (IM)	92.7	7.3	-	-	-	-	8.1

* $Mg_{0.98}Ni_{0.02}Al_2O_4$

** $Mg_{0.97}Ni_{0.03}Al_2O_4$

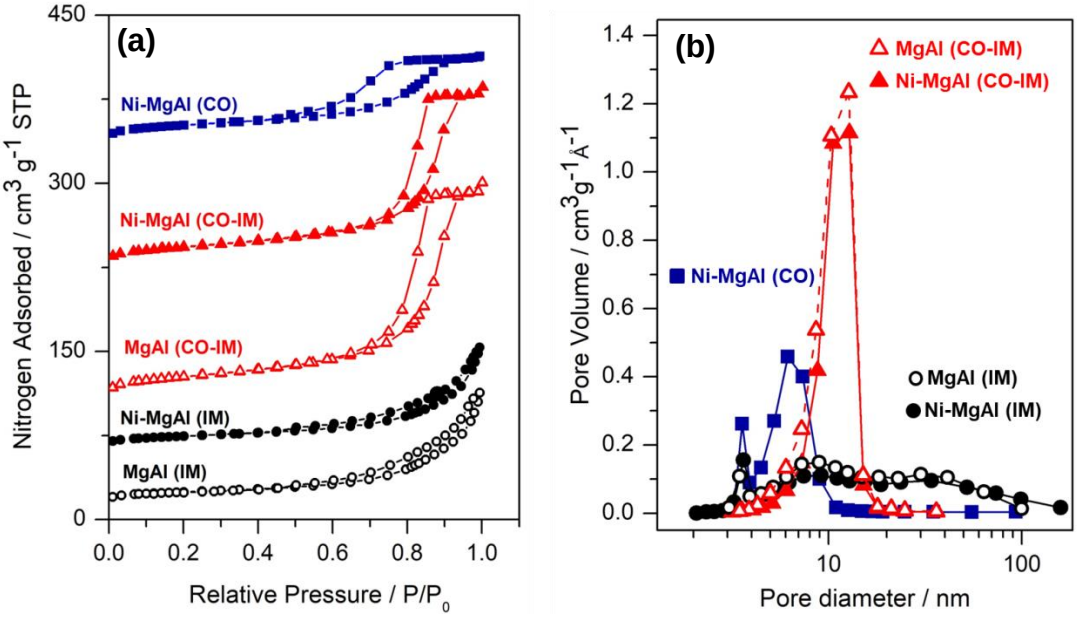

Figure 1. Nitrogen adsorption-desorption isotherms (a) and pore size distribution (b) of support and Ni-catalysts.

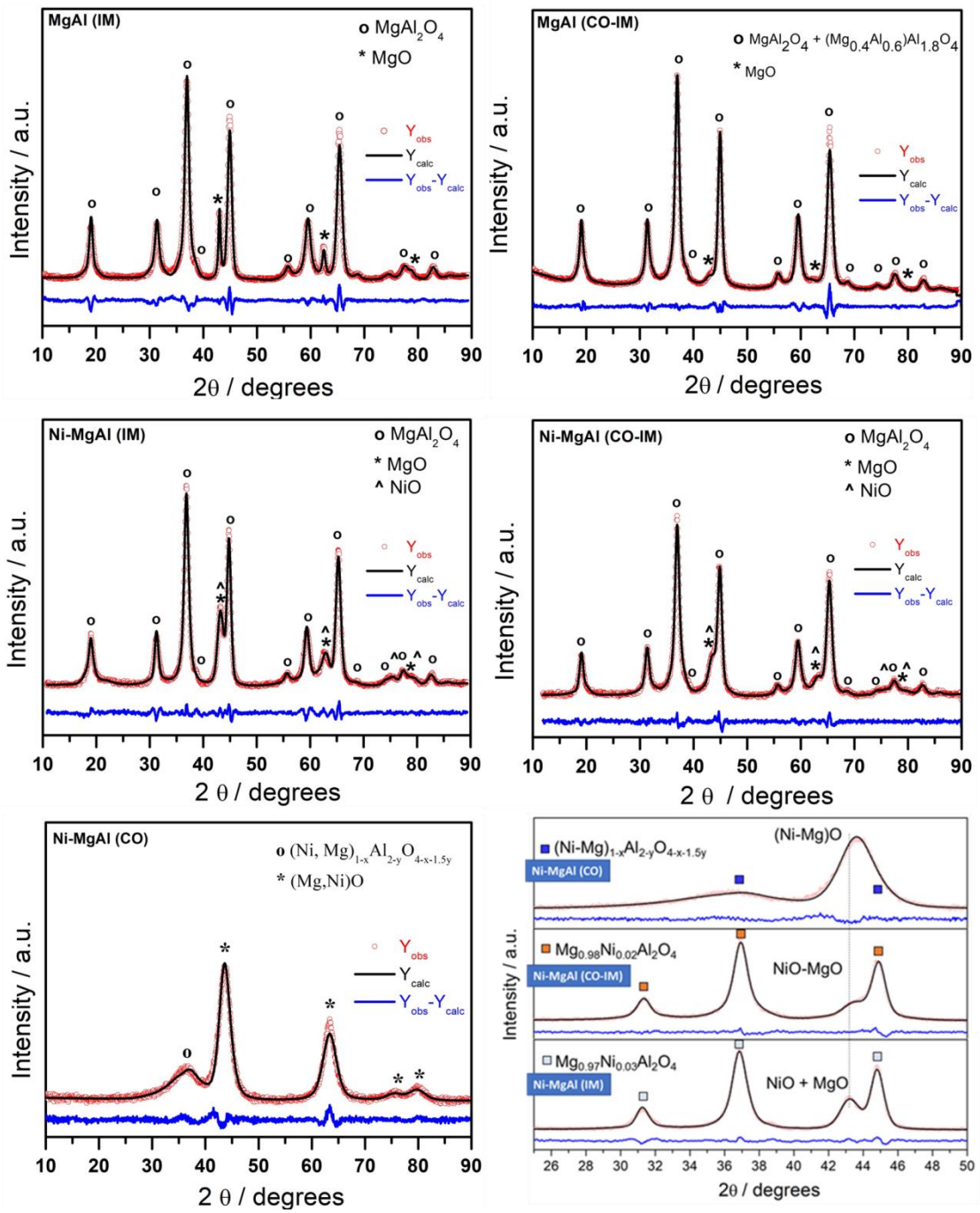

Figure 2. Experimentally observed (dots), Rietveld calculated (continuous line) and difference (continuous bottom line) profiles for calcined supports and catalysts obtained after Rietveld analysis of the XRD data. A zoom comparative of the three catalysts in the 25-50 degrees region is included.

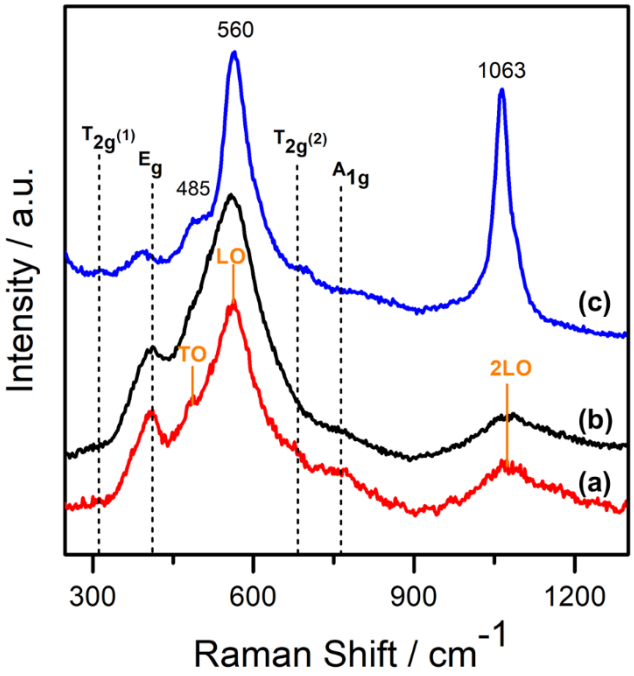

Figure 3. Raman spectra of the catalysts prepared by different methods: (a) Ni-MgAl (CO-IM), (b) Ni-MgAl (IM), and (c) Ni-MgAl (CO).

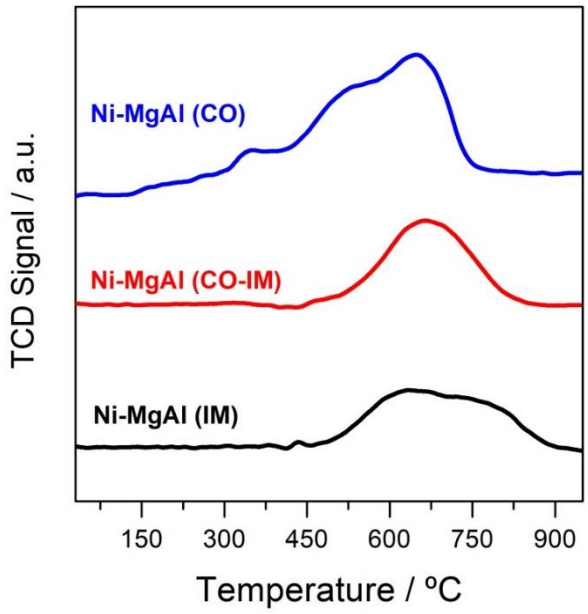

Figure 4. H_2-TPR profiles of Ni catalysts prepared by different methods.

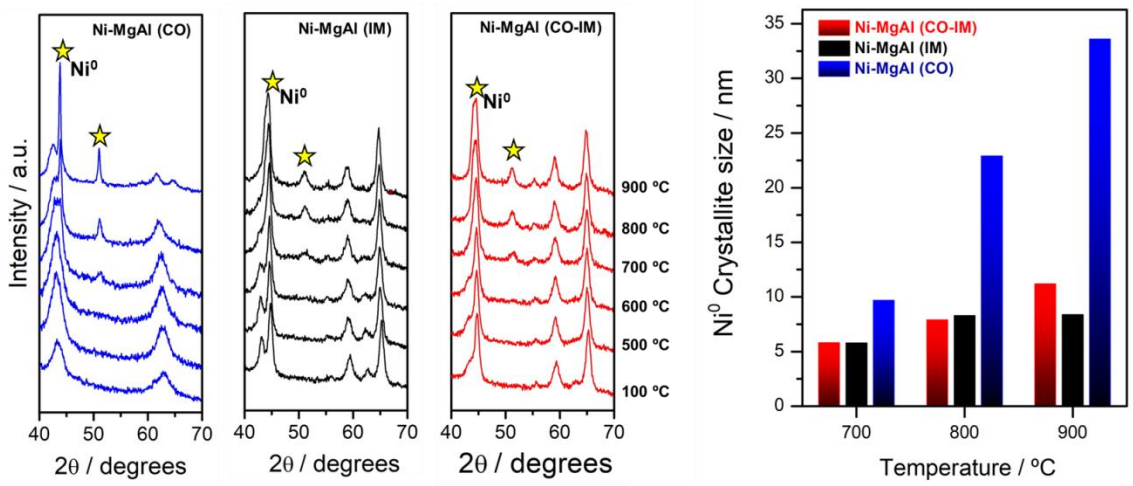

Figure 5. (a) Evolution of XRD patterns (☆Niº JCPDS 00-004-0850) and (b) metallic nickel crystallite sizes estimated during the reduction pretreatment in 5% v/v H_2/N_2 flow as function of temperature in the prepared catalysts.

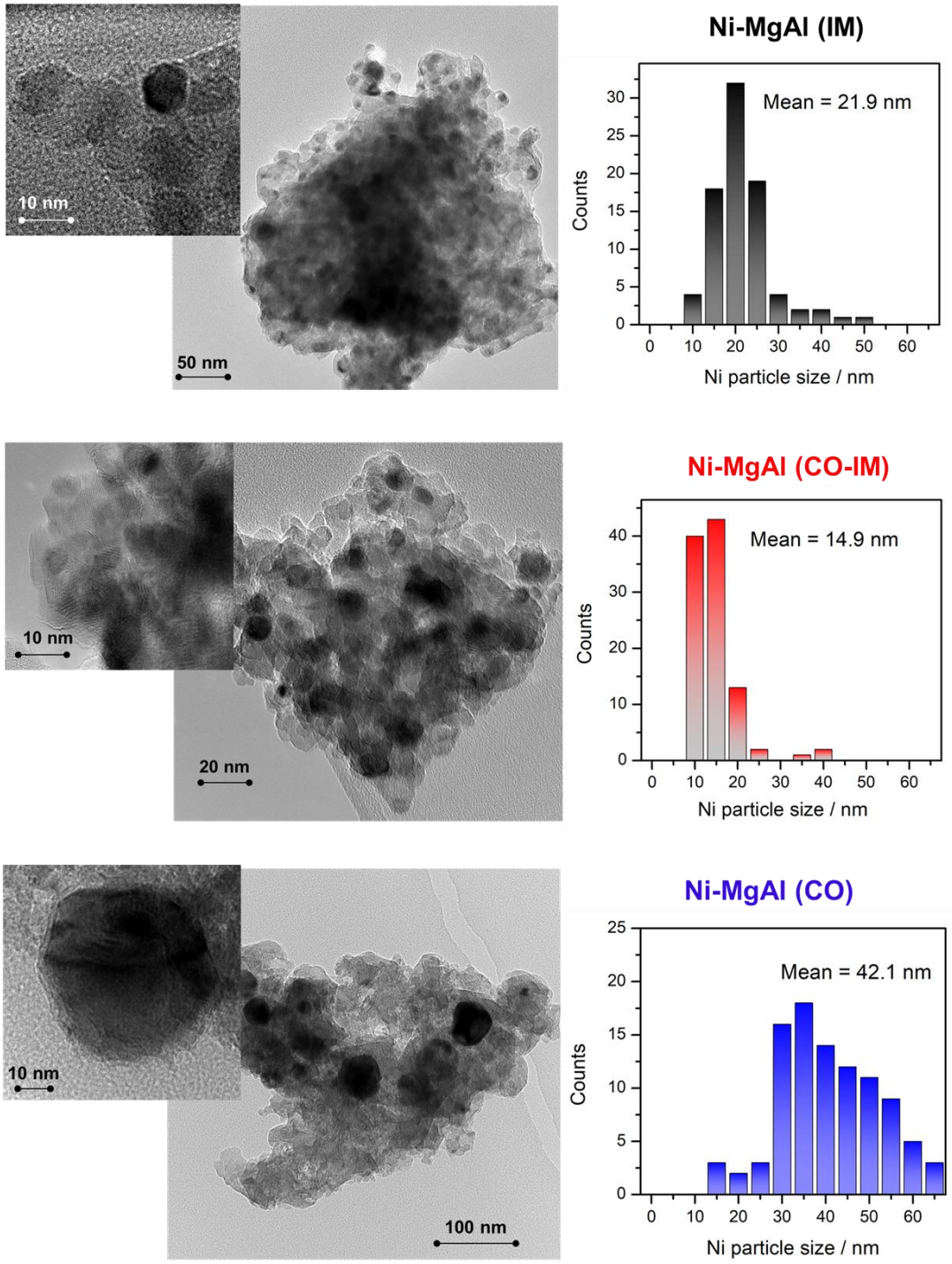

Figure 6. Selected HR-TEM micrographs and distribution histograms of nickel particles of the reduced catalysts prepared using different methods.

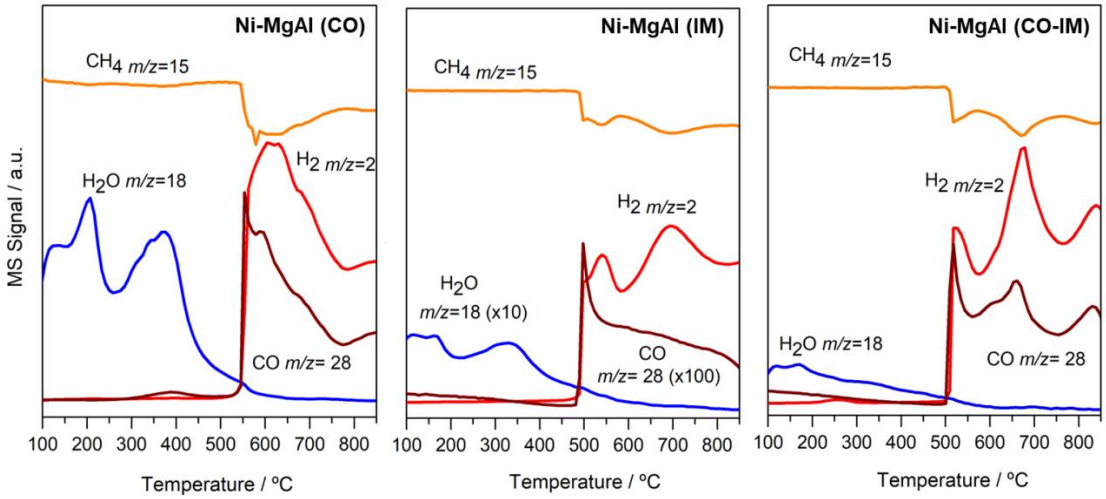

Figure 7. CH_4-TPSR profiles of Ni catalysts prepared by different methods.

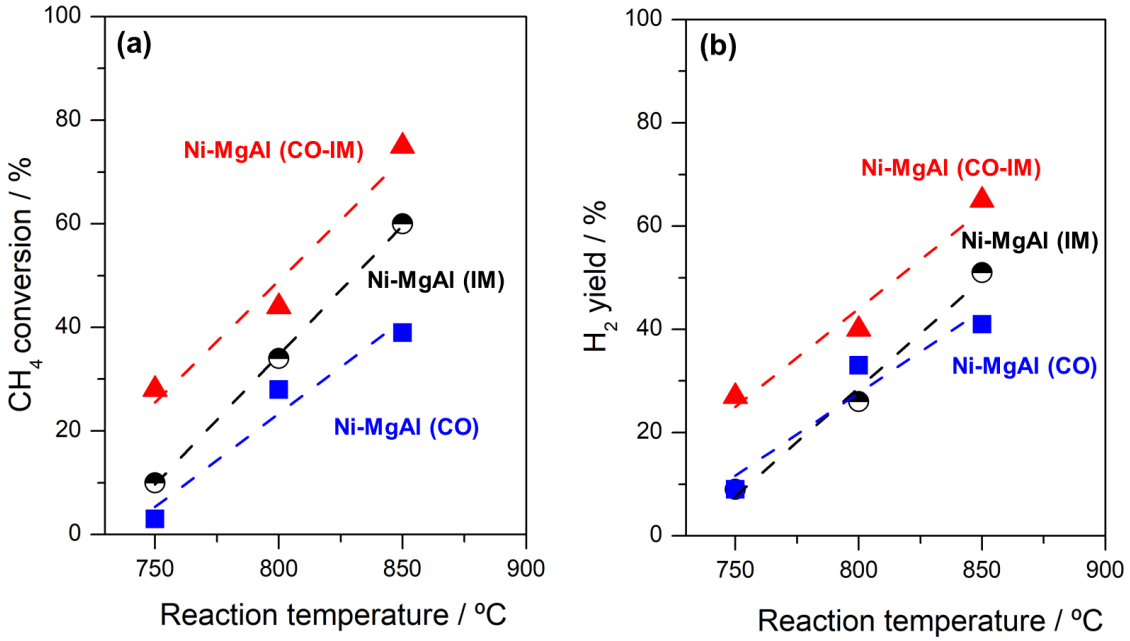

Figure 8. Methane conversion (a) and yield to H_2 (b) varying with the reaction temperature for atmospheric pressure methane steam reforming at GHSV of 60 L g^{-1} h^{-1} and steam-to-carbon ratio of 1.24 over Ni-Mg-Al catalysts prepared by different methods.

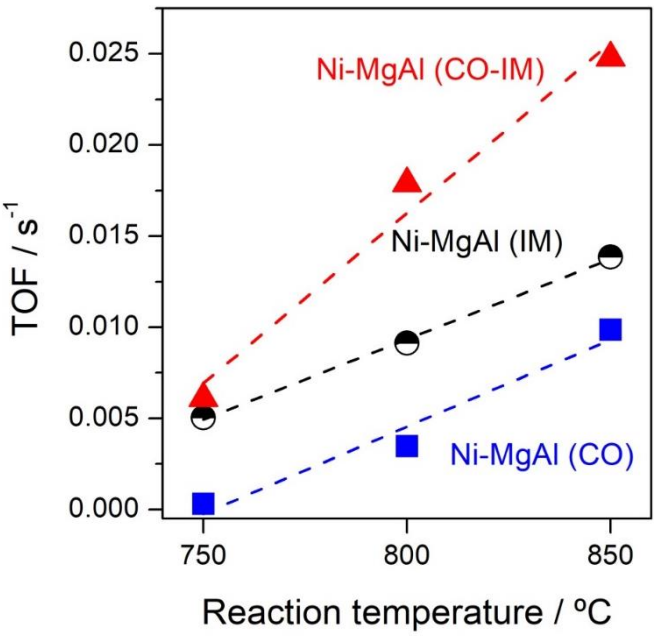

Figure 9. TOF´s of the prepared catalysts as function of the reaction temperature for atmospheric pressure methane steam reforming at GHSV of 60 L g^{-1} h^{-1} and steam-to-carbon ratio of 1.24.

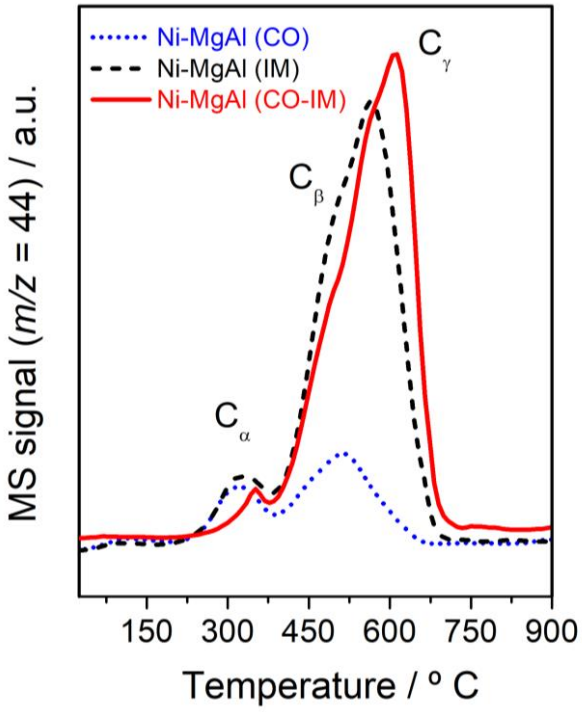

Figure 10. TPO profiles of spent catalysts after steam reforming of methane reaction.

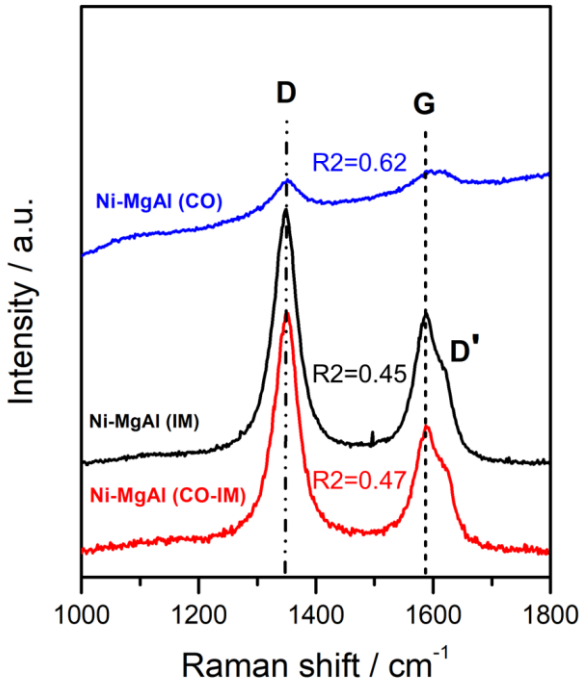

Figure 11. Raman spectra of spent catalysts after methane steam reforming reaction.